Structural, electronic, thermodynamic and optical properties of alkaline earth oxides MgO, SrO and their alloys

6 authors, including:

Malika Labidi
Institut Supérieur des Technologies de l'Environnement
21 PUBLICATIONS   112 CITATIONS

Salima Labidi
Badji Mokhtar - Annaba University
27 PUBLICATIONS   170 CITATIONS

Ghemid Sebti
78 PUBLICATIONS   542 CITATIONS

Hocine Meradji
Badji Mokhtar - Annaba University
99 PUBLICATIONS   644 CITATIONS

Some of the authors of this publication are also working on these related projects:

Project   Half-Metallic Ferromagnetism in cubic perovskite compounds. View project

Project   Half-Metallic Ferromagnetism in New Chalcopyrite Materials. View project

Structural, electronic, thermodynamic and optical properties of alkaline earth oxides MgO, SrO and their alloys

M Labidi[1]**, S Labidi**[1]**, S Ghemid**[1]**, H Meradji**[1] **and F El Haj Hassan**[2]

[1] Laboratoire de Physique des Rayonnements, Département de Physique, Faculté des Sciences, Université de Annaba, Algeria
[2] Laboratoire de Physique des Matériaux, Faculté des Sciences (1), Université Libanaise, Elhadath, Beirut, Lebanon

E-mail: hmeradji@yahoo.fr

Abstract

The structural, electronic, optical and thermodynamic properties of $Mg_{1-x}Sr_xO$ ternary alloys in NaCl structures at various Sr concentrations are presented. The calculations were performed using the full potential linearized augmented plane wave (FP-LAPW) method within the density functional theory (DFT) in the local density approximation (LDA) and two developed refinements, namely the generalized gradient approximation (GGA) of Perdew *et al* (1996 *Phys. Rev. Lett*. **77** 3865) for the structural properties and Engel and Vosko (1993 *Phys. Rev*. B **47** 13164) for the band structure calculations. Deviation of the lattice constants from Vegard's law and the bulk modulus from the linear concentration dependence (LCD) were observed for the alloys. The microscopic origins of the gap bowing were explained by using the approach of Bernard and Zunger (1986 *Phys. Rev. Lett*. **34** 5982). The refractive index and optical dielectric constant for the alloys of interest were calculated by using different models. In addition, the thermodynamic stability of the alloys was investigated by calculating the critical temperatures of alloys.

PACS numbers: 61.66.Dk, 71.15.Mb, 71.15.Nc, 71.20.Nr, 71.22.+i, 78.20.Ci

1. Introduction

MgO and SrO represent two II–VI compounds crystallizing in the rocksalt structure with insulating characteristics, such as large band gaps, and semiconducting characteristics (large valence band widths). These oxides have been considered as a typical case for understanding bonding in ionic oxides and are also one of the most fundamental materials for industrial sciences. This is because of their wide range of applications, ranging from catalysis to microelectronics. For example, their catalytic properties are important for chemical engineering [1].

MgO has been the subject of some parameter-free self-consistent band structure calculations [1–5] and SrO has been studied in many experimental and theoretical works. Taurian *et al* [6] studied the electronic structure with the linearized-muffin-tin orbital (LMTO) method. Pandey *et al* [7] calculated the electronic structure following the

Adams–Gilbert–Kunz (AGK) localized-orbital Hartree–Fock method. Zhang and Bokowinski [8] calculated the transition pressure using a modified-electron gas model. It was expected that the band gap (7.8) of MgO [9] can be modulated to 5.71 eV by alloying with SrO, a mixture of MgO (direct band gap) and SrO (indirect band gap), which is interesting for the optical properties and can cover green and blue to UV light spectra [10].

To provide further insight into the nature of these materials, we present the results of *ab initio* calculations of MgO and SrO compounds and their ternary alloys $Mg_{1-x}Sr_xO$ in rocksalt structure. In this work, we focus our attention on the study of variations in structural, electronic and thermodynamic parameters such as the lattice constant, bulk modulus and band-gap energy. This study was carried out using the full potential linearized angmented plane ware (FP-LAPW) [11] method. The crossover concentration of the indirect-to-direct band gap has also been explored. In addition

to the FP-LAPW method, the composition dependence of the refractive index and dielectric constant was studied by using different models.

Having introduced the problem, we give a description of computational method in the following section. In section 3, the results and discussion for the structural, electronic and thermodynamic properties of $Mg_{1-x}Sr_xO$ alloy are given. Section 4 summarizes the paper and gives the conclusion.

2. Method of calculation

The calculations presented in this work were performed using the FP-LAPW method. By this method no shape approximation on the potential or on the electronic charge density is made. Inside atomic spheres, a linear combination of radial functions times spherical harmonics is used, while in the interstitial region a plane wave expansion is used. The method is implemented in WIEN2K code [11], which allows the inclusion of local orbitals in the basis in order to improve the linearization and make possible a consistent treatment of semicore and valence states in an energy window. We used both local density approximation (LDA) and generalized gradient approximation (GGA). The exchange-correlation potential for the structural properties was calculated by GGA based on the Perdew *et al* [12] form, while for the optical and electronic properties, the exchange-correlation functional of Engel and Vosko (EV-GGA) [13] was applied. In the calculation, the convergence parameter RK_{max}, which controls the size of the basis sets in these calculations, was set as 8.0. The cut-off energy, which defines the separation between the core and valence states, was set as -6.0 Ry. For the sphere radii, we have adopted the values of 1.9, 2.0 and 1.9 au for Mg, Sr and O, respectively. A mesh of 47 special *k*-points for binary compounds and 125 special *k*-points for the alloy were taken in the irreducible wedge of the Brillouin zone. The lattice structures of the alloys under investigation have been modeled at selected compositions as detailed in our previous work [14].

3. Results and discussion

3.1. Structural properties

The ground state bulk properties of the crystals were obtained using the calculations of the total energy as a function of unit cell volume.

Our calculated values for the equilibrium lattice constant a and the bulk modulus B for the binary compounds are summarized in table 1 together with the available experimental [15–17, 21] and theoretical [18–20] data. The values of the lattice parameters a are in very good agreement with the measured values. In the present calculation, we have used LDA and GGA. LDA overestimates the bulk modulus and underestimates the equilibrium lattice constant, while GGA gives a large lattice constant but a smaller bulk modulus. Figure 1 shows the variation of the calculated equilibrium lattice constant versus concentration for the $Mg_{1-x}Sr_xO$ alloy. A large deviation from Vegard's law [22] is clearly visible for the $Mg_{1-x}Sr_xO$ alloy with upward bowing parameters equal to -0.523 and -0.531 Å with GGA and LDA, respectively,
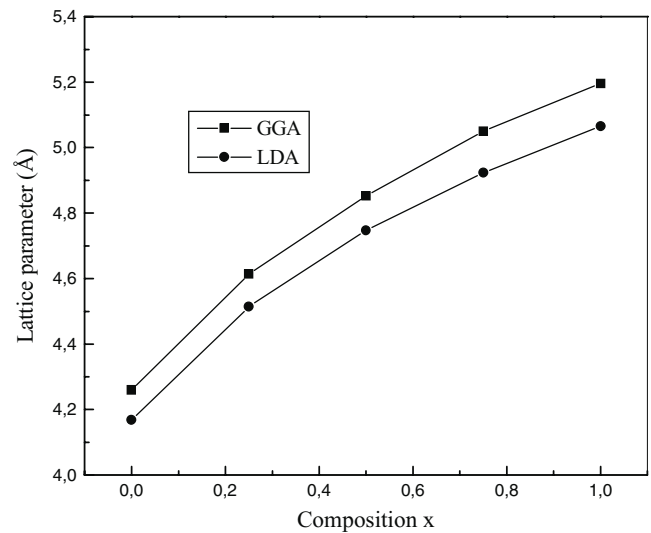
Figure 1. Calculated equilibrium lattice constants of the $Mg_{1-x}Sr_xO$ alloy for different concentrations using LDA and GGA.
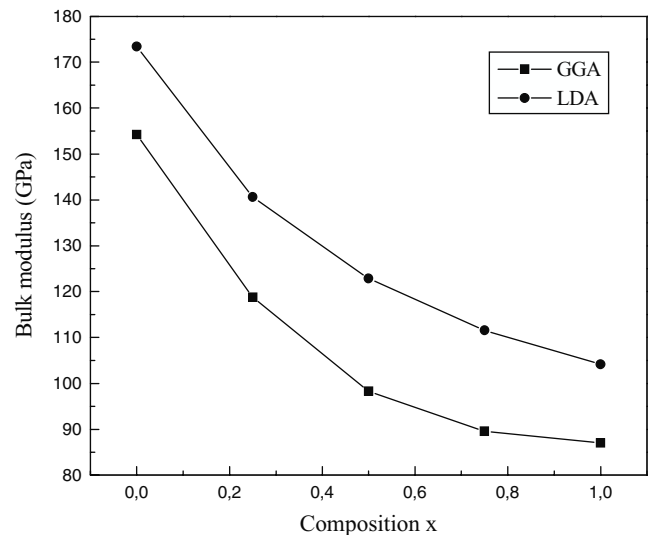
Figure 2. Calculated bulk modulus of the $Mg_{1-x}Sr_xO$ alloy for different concentrations using LDA and GGA.

obtained by fitting the calculated values with a polynomial function. Usually, in the treatment of alloy problems, it is assumed that the atoms are located at the ideal sites and the lattice constants of alloys should vary linearly with composition x according to Vegard's law; however, violations of Vegard's rule have been reported in semiconductor alloys both experimentally [23] and theoretically [24]. The physical origin of this large deviation from Vegard's law should be mainly due to the large mismatch of the lattice constants of MgO and SrO compounds. Also, it should be related to the size of atoms, the ratio $R(Sr)/R(Mg) = 0.51$, where R is the atomic radius. It can be noted that this ratio is smaller if the magnesium atom is substituted by the strontium one. Our results indicate that this violation of Vegard's law has a significant effect on the optical bowing parameter as shown in the next section.

Figure 2 shows the bulk modulus as a function of x for the $Mg_{1-x}Sr_xO$ alloy. A significant deviation from the linear concentration dependence (LCD) with downward bowing

Table 1. The calculated lattice parameter and bulk modulus of MgO and SrO compounds and their alloy.

	x	Lattice constant a (Å)				Bulk modulus B (GPa)			
		This work		Experiment	Other calculations	This work		Experiment	Other calculations
		LDA	GGA			LDA	GGA		
$Mg_{1-x}Sr_xO$	0	4.168	4.260	4.213[a], 4.212[b]	4.259[d], 4.247[e], 4.261[f]	173.40	154.24	156[g]	160[d], 169.1[e], 161.9[f]
	0.25	4.514	4.614			140.61	118.74		
	0.5	4.747	4.853			122.86	98.31		
	0.75	4.923	5.050			111.54	89.54		
	1	5.065	5.196	5.16[c]	5.197[d]	104.11	86.96	91[c]	86[d]

[a] Fei [15].
[b] Spexil *et al* [16].
[c] Liu and Bassett [17].
[d] Tsuchiya *et al* [18].
[e] Jaffe *et al* [19].
[f] Amrani *et al* 20].
[g] Mao and Bell [21].

Table 2. The gap energy E_g of the $Mg_{1-x}Sr_xO$ ternary alloy at equilibrium volume (all the values are in eV).

	x	$\Gamma \to \Gamma$					$\Gamma \to x$				
		This work			Experiment	Other works	This work			Experiment	Other works
		LDA	GGA	EVGGA			LDA	GGA	EVGGA		
$Mg_{1-x}Sr_xO$	0	4.968	4.431	5.419	7.8[a]	4.98[b], 4.5[c], 5.05[d]	6.167	9.115	10.414		8.96[d]
	0.25	2.125	1.998	2.868			4.956	4.782	5.454		
	0.5	1.876	1.787	2.513			4.141	3.758	4.480		
	0.75	2.188	1.967	2.551			4.212	3.907	4.297		
	1	4.139	4.300	5.053	5.90[e]	4.42[d]	3.120	3.335	4.090	5.71[f]	3.01[d]

[a] Whited [9].
[b] Stypanyuk *et al* [26].
[c] Chang and Cohen [27].
[d] Baltache *et al* [28].
[e] Rao and Kearney [29].
[f] Zollweg [30].

equal to 88.5 and 65.3 GPa with GGA and LDA, respectively, was observed. This large deviation is mainly due to the large mismatch of the bulk modulus of SrO and MgO binary compounds.

3.2. Band structures

Knowledge of the energy band structures provides valuable information on its potential utility in fabricating electronic devices. It is also well known that in the electronic band structure calculations within density functional theory (DFT), both LDA and GGA usually underestimate the energy band gap [25]. This is mainly due to the fact that they have simple forms that are not sufficiently flexible to accurately reproduce both the exchange-correlation energy and the corresponding potential. Here, we have tried the EVGGA along with the standard LDA and GGA for the band structure calculations. Calculated results on the direct and indirect band gaps for MgO, SrO and their alloys using LDA, GGA and EVGGA are summarized in table 2, along with the experimental values and those obtained by other theoretical calculations for the binary compounds, but in the case of alloys there are no theoretical or experimental values to compare with. It is clearly seen that the results calculated using EVGGA are in reasonable agreement with experiment, whereas LDA

and GGA give lower values. EVGGA reproduces a better exchange potential at the cost of less accuracy in exchange energy. For this reason, EVGGA presents better results for band-gap energy and other properties that depend primarily on exchange potential.

In the present work, band structure calculations give a direct gap ($\Gamma \to \Gamma$) for the MgO compound and an indirect gap ($\Gamma \to X$) for SrO. Hence, one can expect that the band gap of the $Mg_xS_{1-x}O$ alloy should undergo an indirect-to-direct crossover at a certain value of x. For this purpose, we have calculated the indirect ($\Gamma \to X$) and direct ($\Gamma \to \Gamma$) band gaps of the alloy at various concentrations (table 2). Following our earlier works ([31–33]; [34] and references therein; [35]), calculated band-gap energy values at different concentrations were fitted by a second-order polynomial. The results shown in figure 3 are summarized below:

$$Mg_{1-x}Sr_xO \ (\Gamma \to \Gamma)$$

$$\Rightarrow \begin{cases} E_g^{LDA}(x) = 4.83 - 12.24x + 11.59x^2, \\ E_g^{GGA}(x) = 4.373 - 11.45x + 11.34x^2, \\ E_g^{EVGGA}(x) = 5.39 - 12.41x + 11.99x^2, \end{cases}$$

$$\tag{1}$$
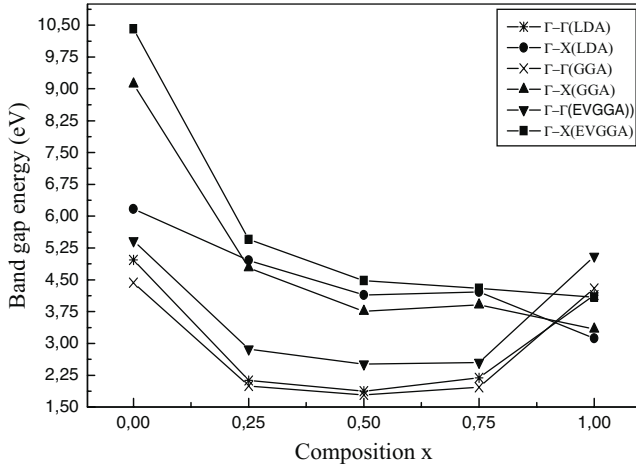
Figure 3. Direct and indirect band-gap energies of the $Mg_{1-x}Sr_xO$ alloy as a function of Sr concentrations using LDA, GGA and GGA-EV.

$Mg_{1-x}Sr_xO$ ($\Gamma \to X$)

$$\Rightarrow \begin{cases} E_g^{LDA}(x) = 6.05 - 4.02x + 1.28x^2, \\ E_g^{GGA}(x) = 8.71 - 14.91x + 9.94x^2, \\ E_g^{EVGGA}(x) = 9.97 - 17.29x + 11.76x^2. \end{cases} \quad (2)$$

Figure 3 shows the band gap versus Sr concentration at Γ and X points for the $Mg_{1-x}Sr_xO$ alloy. From figure 3, it is clear that the crossover from indirect band gap ($\Gamma \to X$) to direct band gap ($\Gamma \to \Gamma$) is at a concentration of 0.91.

Overall the band-gap bowing parameter of $Mg_{1-x}Sr_xO$ alloys has also been calculated by the equations of Bernard and Zunger ([36] and references therein) for $x = 0.5$. Since the compositional effect on the bowing is considered to be small, the band-gap bowing equations of Bernard and Zunger have been defined only by the contributions of the volume deformation (b_{VD}), the charge transfer (b_{CE}) and the structural relaxation (b_{SR}) of the alloys, as follows:

$$b = b_{VD} + b_{CE} + b_{SR}, \quad (3)$$

$$b_{VD} = 2\left[\varepsilon_{AB}(a_{AB}) - \varepsilon_{AB}(a) + \varepsilon_{AC}(a_{AC}) - \varepsilon_{AC}(a)\right], \quad (4)$$

$$b_{CE} = 2\left[\varepsilon_{AB}(a) + \varepsilon_{AC}(a) - 2\varepsilon_{ABC}(a)\right], \quad (5)$$

$$b_{SR} = 4\left\lfloor \varepsilon_{ABC}(a) - \varepsilon_{ABC}(a_{eq})\right\rfloor. \quad (6)$$

Here, a_{AB}, a_{AC} and a_{eq} are the equilibrium lattice constants of MgO, SrO and $Mg_{1-x}Sr_xO$ alloys, respectively. In the equations, the corresponding lattice constant is used to calculate the energy gap (ε) for the compounds and alloys. Different contributions to the direct gap bowing ($\Gamma \to \Gamma$) were calculated using LDA, GGA and EVGGA schemes and the results are given in table 3. It can be seen that the calculated quadratic parameters (gap bowing) within LDA, GGA and EVGGA are very close to their corresponding results obtained by the Zunger approach. Therefore, the band-gap bowing mainly originates from the charge transfer in

the alloys due to the large electronegativity difference between Sr (0.95) and Mg (1.31) atoms. The small contribution of structural relaxation to the bowing parameter shows that definition of the alloys in the disordered structure model of the atoms is not necessary. The positive small contribution of volume deformation is due to the mismatch of the lattice constants of SrO and MgO.

3.3. Optical properties

Optical properties of a solid are usually described in terms of the complex dielectric function $\varepsilon(\omega) = \varepsilon_1(\omega) + i\varepsilon_2(\omega)$. The imaginary part of the dielectric function in the long wavelength limit has been obtained directly from the electronic structure calculation, using the joint density of states and the optical matrix elements. The real part of the dielectric function can be derived from the imaginary part by the Kramers–Kronig relationship. Knowledge of both the real and the imaginary parts of the dielectric function allows the calculation of important optical functions. The refractive index $n(\omega)$ is given by

$$n(\omega) = \left[\frac{\varepsilon_1(\omega)}{2} + \frac{\sqrt{\varepsilon_1^2(\omega) + \varepsilon_2^2(\omega)}}{2}\right]^{1/2}. \quad (7)$$

At low frequency ($\omega = 0$), we obtain the following relation:

$$n(0) = \varepsilon^{1/2}(0). \quad (8)$$

The refractive index of semiconducting materials is very important in determining the optical and electric properties of the crystal. It is a measure of the transparency of the insulator to incident spectral radiation. In addition, knowledge of the refractive index is essential for devices such as photonic crystals, wave guides, solar cells and detectors [37]. Advanced applications of these alloys can significantly benefit from accurate index data. The use of fast non-destructive optical techniques for epitaxial layer characterization (determination of thickness or alloy composition) is limited by the accuracy with which refractive indices can be related to alloy composition. These applications require an analytical expression of known accuracy to relate the wavelength dependence of the refractive index to alloy composition, as determined from simple techniques such as photoluminescence. In the present study, the refractive index has been obtained using different models that are related to the fundamental energy band gap. The following models are used:

(i) The Moss formula [38] based on the atomic model

$$E_g n^4 = k, \quad (9)$$

where E_g is the energy band gap and k a constant. The value of k is given as 108 eV by Ravindra and Srivastava [38].

(ii) The expression proposed by Ravindra *et al* [39]

$$n = \alpha + \beta E_g, \quad (10)$$

with $\alpha = 4.084$ and $\beta = -0.62\,eV^{-1}$.

4

Table 3. Decomposition of the optical bowing into volume deformation (VD), charge exchange (CE) and structural relaxation (SR) contributions compared with that obtained by a quadratic fit and other predictions (all the values are in eV).

		This work					
		Zunger approach			Quadratic fits		
		LDA	GGA	EVGGA	LDA	GGA	EVGGA
$Mg_{1-x}Sr_xO$	b_{VD}	0.114	0.694	0.934			
	b_{CE}	9.7	8.306	8.834			
	b_{SR}	0.896	0.992	1.124			
	b	10.71	9.992	10.892	11.598	11.340	11.998

Table 4. Refractive indices of $Mg_{1-x}Sr_xO$ for different compositions x.

	x	This work				Experiment	Other calculations
		FP-LAPW	Relation (9)	Relation (10)	Relation (11)		
$Mg_{1-x}Sr_xO$	0	1.685	2.222	1.337	2.004	1.71[a], 1.736[b]	
	0.25	1.888	2.711	2.845	2.711		
	0.5	1.962	2.788	2.976	2.806		
	0.75	1.969	2.722	2.864	2.724		
	1	1.911	2.238	1.418	2.029	1.80[c,d]	1.84[e]

[a]Ho [41].

[b]Lide [42].

[c]Reddy *et al* [43].

[d]Moss *et al* [44].

[e]Salem [45].

(iii) Herve and Vandamme's empirical relation [40] given by

$$n = \sqrt{1 + \left(\frac{A}{E_g + B}\right)^2} \qquad (11)$$

with $A = 13.6$ eV and $B = 3.4$ eV.

In table 4, we summarize the calculated values of the refractive index for the alloys under investigation for some compositions obtained by using the FP-LAPW method and different models. Comparison with the known data has been made where possible. As compared with the other relations used, it appears that the values of the refractive index obtained from FP-LAPW calculations for the end-point compounds (i.e. MgO and SrO) are in better agreement with available experimental results. Due to lack of both experimental and theoretical data in the literature on n of $Mg_{1-x}Sr_xO$ in the composition range $0 < x < 1$, the present results represent reliable predictions of the refractive index.

Figure 4 shows the variation of the calculated refractive index versus concentration for the $Mg_{1-x}Sr_xO$ alloy. The variation is not monotonic. As can be seen, nonlinear behavior of the refractive index can be clearly noticed for all the used methods. This nonlinearity with respect to x obtained in our results arises from the effects of alloy disorder. The calculated refractive indices versus concentration were fitted by a polynomial equation. The results are summarized as follows:

$Mg_{1-x}Sr_xO$

$$\Rightarrow \begin{cases} n_1(x) = 1.692 + 0.886x - 0.673x^2 \text{ (FP-LAPW)}, \\ n_2(x) = 2.229 + 2.404x - 2.387x^2 \text{ (from relation (9))}, \\ n_3(x) = 1.373 + 7.102x - 7.029x^2 \text{ (from relation (10))}, \\ n_4(x) = 2.016 + 3.432x - 3.406x^2 \text{ (from relation (11))}. \end{cases}$$

(12)
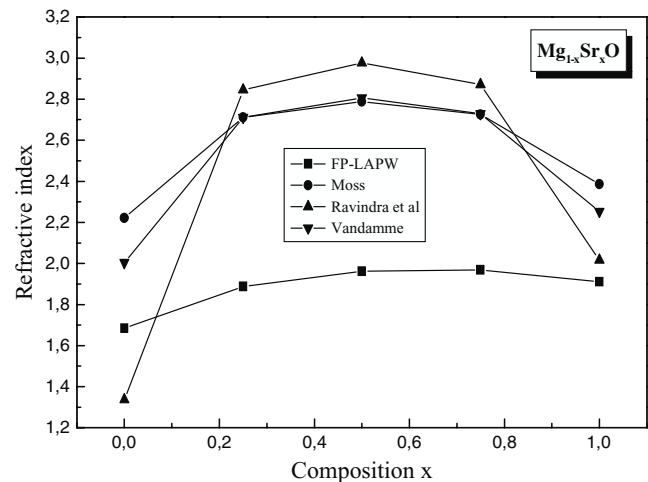
Figure 4. Refractive index for the $Mg_{1-x}Sr_xO$ alloy for different compositions x.

Here $n_1(x)$, $n_2(x)$, $n_3(x)$ and $n_4(x)$ are referred to as the refractive indices obtained from the FP-LAPW method and relations (9)–(11), respectively. For the $Mg_{1-x}Sr_xO$ alloy, an important upward bowing is observed for $n_2(x)$, $n_3(x)$ and $n_4(x)$ compared to $n_1(x)$.

Based on the calculated values of n, the optical dielectric constant as estimated according to expression (8), the results are given in table 5.

It also seems that the FP-LAPW method allows us to obtain values for ε that are in better agreement with experiment when compared with the other models used. This is clearly seen in table 5 for the parent compounds. The agreement with the theoretical results is also good. Qualitatively, the compositional dependence of the dielectric function of the alloys shows the same trend as that of the refractive index. This is not surprising as the dielectric function is directly calculated from relation (8). A least-squares fit was made on

Table 5. Optical dielectric constants of $Mg_{1-x}Sr_xO$ for different compositions x.

	x	This work				Experiment	Other calculations
		FP-LAPW	Relation (9)	Relation (10)	Relation (11)		
$Mg_{1-x}Sr_xO$	0	2.840	4.937	1.788	4.016	2.96[a,b], 3.20[c]	3.02[d]
	0.25	3.564	7.350	8.094	7.350		
	0.5	3.850	7.773	8.857	7.874		
	0.75	3.877	7.409	8.205	7.421		
	1	3.651	5.011	2.010	4.119	3.46[a,b]	3.48[d]

[a]Galtier [46].
[b]Sangster *et al* [47].
[c]Samsonov [48].
[d]Wu and Ceder [49].

the data we obtained, giving the following relations:

$Mg_{1-x}Sr_xO$

$$\Rightarrow \begin{cases} \varepsilon_1(x) = 2.860 + 3.241x - 2.467x^2 \text{ (FP-LAPW)}, \\ \varepsilon_2(x) = 4.967 + 11.978x - 11.896x^2 \text{ (from relation (9))}, \\ \varepsilon_3(x) = 1.905 + 30.412x - 30.190x^2 \text{ (from relation (10))}, \\ \varepsilon_4(x) = 4.065 + 16.395x - 16.284x^2 \text{ (from relation (11))}. \end{cases}$$
$$(13)$$

where $\varepsilon_1(x)$, $\varepsilon_2(x)$, $\varepsilon_3(x)$ and $\varepsilon_4(x)$ stand for the optical dielectric constants estimated from the corresponding refractive indices $n_1(x)$, $n_2(x)$, $n_3(x)$ and $n_4(x)$, respectively, for a given value of x.

3.4. Thermodynamic properties

In order to study the phase stability of the $Mg_{1-x}Sr_xO$ alloy, we calculated the phase diagram based on the regular-solution model [50–52]. For alloys, the Gibbs free energy of mixing ΔG_m is expressed as

$$\Delta G_m = \Delta H_m - T \Delta S_m, \quad (14)$$

where

$$\Delta H_m = \Omega x(1-x), \quad (15)$$

$$\Delta S_m = -R [x \ln x + (1-x) \ln (1-x)]. \quad (16)$$

ΔH_m and ΔS_m are the enthalpy and entropy of mixing, respectively; Ω is the interaction parameter and depends on the material; R is the gas constant and T the absolute temperature. The mixing enthalpy of alloys can be obtained from the calculated total energies as $\Delta H_m = E_{AB_xC_{1-x}} - xE_{AB} - (1-x)E_{AC}$, where $E_{AB_xC_{1-x}}$, E_{AB} and E_{AC} are the respective energies of the AB_xC_{1-x} alloy and the binary compounds AB and AC. We then calculated ΔH_m to obtain Ω as a function of concentration. The interaction parameter increases almost linearly with increasing x. From a linear fit we obtained

$$Mg_{1-x}Sr_xO \Rightarrow \Omega \left(kcal\, mol^{-1} \right) = 47.4 - 28.8x. \quad (17)$$

First we calculate ΔG_m using equations (14)–(16). Then we use the Gibbs free energy at different concentrations to calculate the T–x phase diagram, which shows the stable,
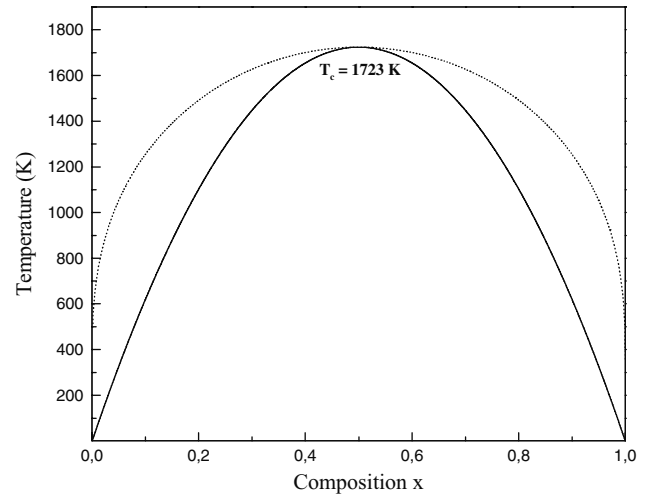
Figure 5. T–x phase diagram of the $Mg_{1-x}Sr_xO$ alloy. Dashed line: binodal curve; solid line: spinodal curve.

metastable and unstable mixing regions of the alloy. At a temperature lower than the critical temperature T_c, the two binodal points are determined as those points at which the common tangent line touches the ΔG_m curves. The two spinodal points are determined as those points at which the second derivative of ΔG_m is zero; $\partial^2(\Delta G_m)/\partial x^2 = 0$.

Figure 5 shows the calculated phase diagram including the spinodal and binodal curves of the alloy of interest. We observed a critical temperature $T_c = 1723$ K for the $Mg_{1-x}Sr_xO$ alloy. Hence, our results indicate that the alloy $Mg_{1-x}Sr_xO$ is stable at high temperature.

4. Conclusion

We have used the FP-LAPW method to study the structural, electronic and thermodynamic properties of the $Mg_{1-x}Sr_xO$ alloy. The composition dependence of the lattice constants, bulk modulus and band gap has been studied. The calculated band structure shows a transition from indirect to direct band gap $(\Gamma \rightarrow X) \rightarrow (\Gamma \rightarrow \Gamma)$ at $x = 0.91$. Like the lattice constant, the band gap exhibits nonlinear behavior or bowing effect with the change of concentration. The main contribution to the total band-gap bowing parameter comes from the charge transfer effect. We have also computed the refractive index and the dielectric constant; our results for all the used methods showed that the refractive index varies nonlinearly. Finally, we observed a critical temperature $T_c = 1723$ K, which means

that the $Mg_{1-x}Sr_xO$ alloy is stable at high temperature. These data may be useful for mechanical, chemical and electronic industries where the performance of a device is affected by its thermodynamic properties.

References

[1] Chaudhary V R, Rajput A M and Mamman A S 1998 *J. Catal.* **178** 576
[2] Pantelides S, Michish D J and Kunz A B 1974 *Phys. Rev. B* **10** 5203
[3] Walch P F and Ellis D E 1973 *Phys. Rev. B* **8** 5920
[4] Redinger J and Schwarz K 1981 *Z Phys. B* **40** 269
     Christensen N E and Kollar J 1983 *Solid State Commun.* **46** 727
     Koenig C, Christensen N E and Kollar J 1984 *Phys. Rev. B* **29** 6481
[5] Chang K J and Cohen M L 1984 *Phys. Rev. B* **30** 4774
[6] Taurian O E, Springborg M and Christensen N E 1985 *Solid State Commun.* **55** 351
[7] Pandey R, Jaffe J E and Kunz A B 1991 *Phys. Rev. B* **43** 9228
[8] Zhang H and Bukowinski M S T 1991 *Phys. Rev. B* **44** 2495
[9] Whited R C, Flaten C J and Walker W C 1973 *Solid State Commun.* **13** 1903
[10] Ye Z, Ma D, He J, Huang J, Zhao B, Luo X and Xu Z 2003 *J. Cryst. Growth* **256** 78
[11] Blaha P, Schwarz K, Madsen G K H, Kvasnicka D and Luitz J 2001 *WIEN2k, an Augmented Plane Wave Plus Local Orbitals Program for Calculating Crystal Properties* (Vienna, Austria: Vienna University of Technology)
     Madsen G K H, Blaha P, Schwarz K, Sjostedt E and Nordstrom L 2001 *Phys. Rev. B* **64** 195134
     Schwarz K, Blaha P and Madsen G K H 2002 *Comput. Phys. Commun.* **147** 71
[12] Perdew J P, Burke S and Ernzerhof M 1996 *Phys. Rev. Lett.* **77** 3865
[13] Engel E and Vosko S H 1993 *Phys. Rev. B* **47** 13164
[14] El Haj Hassan F, Breidi A, Ghemid S, Amrani B, Meradji H and Pagès O 2010 *J Alloys Compd.* **499** 80
[15] Fei Y 1999 *Am. Mineral.* **84** 272
[16] Spezial S, Zha C S, Duffy T S, Hemley R J and Mao H K 2001 *J. Geophys. Res.* **106** 515
[17] Liu L G and Bassett W A 1972 *J. Geophys. Res.* **77** 4934
[18] Tsuchiya T and Kawamura K 2001 *J. Chem. Phys.* **114** 10086
[19] Jaffe J E, Snyder J A, Lin Z and Hess A C 2000 *Phys. Rev. B* **62** 1660
[20] Amrani B, Ahmed R and El Haj Hassan F 2006 *Comput. Mater. Sci.* **40** 66
[21] Mao H K and Bell P M 1979 *J. Geophys. Res.* **84** 4533
[22] Vegard L 1921 *Z. Phys.* **5** 17
[23] Jobst J, Hommel D, Lunz U, Gerhard T and Landwehr G 1996 *Appl. Phys. Lett.* **69** 97
[24] El Haj Hassan F 2005 *Phys. Status Solidi* b **242** 909
[25] Dufek P, Blaha P and Schwarz K 1994 *Phys. Rev. B* **50** 7279
[26] Stypanyuk V S, Szasz A, Grigorenko B L, Farberovich O V and Kastnelson A A 1989 *Phys. Status Solidi* b **155** 79
[27] Chang K J and Cohen M L 1984 *Phys. Rev. B* **30** 4774
[28] Baltache H, Khenata R, Sahnoun M, Driz M, Abbar B and Bouhafs B 2004 *Physica B* **344** 334
[29] Rao A S and Kearney R J 1979 *Phys. Status Solidi* b **95** 243
[30] Zollweg R J 1958 *Phys. Rev.* **111** 113
[31] El Haj Hassan F and Akbarzadeh H 2005 *Mater. Sci. Eng. B* **121** 170
[32] El Haj Hassan F 2005 *Phys. Status Solidi* b **242** 3129
[33] Baaziz H, Charifi Z, El Haj Hassan F, Hashemifar S J and Akbarzadeh H 2006 *Phys. Status Solidi* b **243** 1296
[34] Charifi Z, El Haj Hassan F, Baaziz H, Khosravizadeh Sh, Hashemifar S J and Akbarzadeh H 2005 *J. Phys.: Condens. Mater* **17** 7077
     Yeo Y C, Chong T C and Li M F 1998 *J. Appl. Phys* **83** 1429
[35] El Haj Hassan F 2005 *Phys. Status Solidi* b **242** 909
[36] Srivastava G P, Martins J L and Zunger A 1985 *Phys. Rev. B* **31** 2561
     Bernard J E and Zunger A 1986 *Phys. Rev. B* **34** 5992
     Zunger A, Wei S H, Ferreira L G and Bernard J E 1990 *Phys. Rev. Lett.* **65** 353
     Wei S H, Ferreira L G, Bernard J E and Zunger A 1990 *Phys. Rev. B* **42** 9622
[37] Ravindra N M, Ganapathy P and Choi J 2007 *Infrared Phys. Technol.* **50** 21
[38] Gupta V P and Ravindra N M 1980 *Phys. Status Solidi* b **10** 715
[39] Ravindra N M, Auluck S and Srivastava V K 2003 *Phys. Status Solidi* b **93** 155
[40] Herve J P L and Vandamme L K J 1994 *Infrared Phys. Technol.* **35** 609
[41] Ho I C 1997 *J. Sol-Gel Sci. Technol.* **9** 295–301
[42] Lide D R 1991 *CRC Handbook of Chemistry and Physics* 71th edn (Boston, MA: CRC Press) pp 4–77
[43] Reddy R R, Kumar M R and Rao T V R 1993 *Infrared Phys.* **34** 103
[44] Moss T S, Burrel G J and Ellis B 1973 *Semiconductor Opto-Electronics* (London: Butterworths)
[45] Salem M A 2003 *Chin. J. Phys.* **41** 288
[46] Galtier M, Montaner A and Vidal G 1972 *J. Phys. Chem. Solids* **33** 2295
[47] Sangster M J L, Peckham G and Saunderson D H 1970 *J. Phys. C: Solid State Phys.* **3** 1026
[48] Samsonov G V 1982 *The Oxide Handbook* 2nd edn (New York: IFI/Plenum) p 212
[49] Wu E J and Ceder G 2001 *J. Appl. Phys.* **89** 15
[50] Swalin R A 1961 *Thermodynamics of Solids* (New York: Wiley)
[51] Ferreira L G, Wei S H, Bernard J E and Zunger A 1999 *Phys. Rev. B* **40** 3197
[52] Teles L K, Furthmuller J, Scolfaro L M R, Leite J R and Bechstedt F 2000 *Phys. Rev B* **62** 2475